J. COMBIN. MATH. COMBIN. COMPUT. 127b (2025) 2949--2969

Journal of Combinatorial Mathematics and Combinatorial Computing
www.combinatorialpress.com/jcmcc

Combinatorial Press

Optimized design study of permanent magnet switch using deep learning fused with finite element analysis

Chunxiao Li[1,✉], Wenxuan Wang[1], Xin Li[1]

[1] State Grid Cangzhou Electric Supply Company, Cangzhou, Hebei, 061000, China

ABSTRACT

Aiming at the problems of unfixed switching frequency and complicated calculation in the control of permanent magnet synchronous motor, a permanent magnet switch FNN-PID control strategy based on deep learning technology is proposed. Based on the vector control of permanent magnet synchronous motor, the resonant pole inverter is combined with permanent magnet switch control, and then the fuzzy neural network and incremental PID algorithm are used to construct the optimization strategy of permanent magnet synchronous motor switching frequency FNN-PID control. And combined with the finite element simulation software, the permanent magnet switch finite element model is constructed, and the effectiveness of the FNN-PID control strategy is illustrated by verifying the permanent magnet switch control strategy and the temperature rise curve change. When using the FNN-PID control strategy, the electromagnetic torque quickly reaches stabilization near the given torque of 9 N-m after 0.03 s of startup, and the permanent magnet switch frequency of the FNN-PID control strategy is reduced by 24.04%. The difference between the measured maximum winding temperature and the calculated maximum temperature under rated operating conditions is less than 9°C, and the permanent magnet switching loss is reduced by about 35% with the FNN-PID control strategy compared with the traditional MTPA control strategy. Therefore, the combination of deep learning technology and finite element analysis can explore the optimization effect of PM switches from the strategy and application dimensions and provide research ideas for the stable operation of PM switches.

Keywords: deep learning, finite element model, fuzzy neural network, incremental PID, FNN-PID, permanent magnet switch

1. Introduction

Permanent magnet switch, also known as permanent magnet controller, permanent magnet drive module, etc., is a kind of electrical switch that is controlled by using the force of permanent magnetic

✉ Corresponding author.
E-mail address: 18031991855@163.com (C. Li).
Received 30 May 2024; Revised 15 August 2024; Accepted 10 January 2025; Published Online 16 April 2025.
DOI: 10.61091/jcmcc127b-166

field, and its working principle is realized based on the interaction between the magnetic field generated by the applied current and the permanent magnetic field, which mainly includes the permanent magnet isolation switch and the permanent magnet limit switch [1]. Distribution network is the end link to ensure the reliability of power supply to users, and transient faults account for most of the distribution network, which is the main factor affecting the quality of power and the reliability of power supply [2]. At present, most of the distribution networks use customer demarcation load switches or circuit breakers to isolate customer faults, and these switch actuators are similar to the line-out circuit breakers, which also use pop-up actuators [3-4]. When a fault occurs on the customer side, even if a demarcation circuit breaker is used, the instantaneous quick-break action time of the switch is usually slower than the action time of the substation outgoing circuit breaker, and it cannot form a graded coordination, so the failure of the customer branch line often leads to the blackout of the whole line [5-6]. While the permanent magnet disconnecting switch action speed, especially after the installation of the user side, the user failure to ensure that do not go out, both to reduce the line blackout, but also to reduce the other users of power outages, and at the same time to protect the line other operating equipment [7-8].

Permanent magnet disconnect switches are widely used in power distribution devices, transmission and distribution equipment, industrial and mining enterprises, rail transportation, wind power, solar energy and other fields of the power system, to improve the reliability and safety of the power system, to ensure the normal operation of the equipment is of great significance [9]. In addition, in coal mine production, the in-use main and deputy shaft hoist is mainly used for lowering and lifting personnel, raw coal, gangue and materials, which is one of the main equipments in coal mine production. And its lifting capacity is usually consistent with the main production of the mine, once it can not operate normally, it will inevitably trigger the mine shutdown, it can be said that the safe and stable operation of the mine hoist is the cornerstone of mining production [10-11]. This shows the important role of coal mine hoist in coal mine production. The speed reducer plays an exceptionally important role in the operation of the mine hoist, and its deceleration point control is an important link in the occurrence of faults or accidents [12-13]. The permanent magnet limit switch is widely used in the deceleration point control of mine hoist because of its advantages of sensitive action and no additional power supply. However, as a new type of switching device, the permanent magnet switch, in practical application, suffers from magnetic degradation of the permanent magnet material due to the influence of temperature, while the permanent magnetic field may degrade or even become demagnetized in long-term use, and has poor adaptability under dynamic loads [14]. Therefore, the permanent magnet switch performance and so on need to be optimized.

In this paper, a permanent magnet synchronous motor switching control strategy based on deep learning and finite element software is proposed. In this strategy, the permanent magnet synchronous motor switching control strategy is established based on the mathematical model of the permanent magnet synchronous motor and the introduction of fuzzy neural network and incremental PID algorithm combined with the resonant pole inverter. Then the motor solution domain model for PM synchronous motor switching control is established and the corresponding boundary conditions are designed. Finally, the effectiveness of the FNN-PID control strategy is verified in terms of the operating state, steady state dynamic performance and average switching frequency, and the variation curve of PM switching temperature rise is explored.

2. Mathematical modeling and switching control of permanent magnet synchronous motors

With the emergence of new generation of permanent magnet materials, such as ferrite and NdFeB, the development of permanent magnet synchronous motor (PMSM) has been greatly promoted. These new permanent magnet materials have the advantages of high permeability and high magnetic energy product, which makes PMSM have stronger performance and stability. In many fields such as industrial drives, electric locomotives, wind power, etc., PMSMs are widely used due to their high efficiency, high control accuracy and low cost.

2.1. Mathematical model of permanent magnet synchronous motor

2.1.1. Coordinate system transformations for PMSMs. At present, the modeling coordinate system of PMSM, in addition to the ABC three-phase natural coordinate system, also includes the commonly used α-β-axis stationary coordinate system and d-q-axis synchronous rotation coordinate system. There exists a certain transformation relationship between the coordinate systems, including the Clark transformation of the stationary coordinate system and the Park transformation of the synchronous rotation coordinate system [15].

Clark transformation, can realize the transformation of three-phase ABC natural coordinate variables to two-phase α-β stationary coordinate variables. Clark transformation formula is:

$$\begin{bmatrix} f_\alpha & f_\beta & f_0 \end{bmatrix}^T = T_{3s/2s}\begin{bmatrix} f_A & f_B & f_C \end{bmatrix}^T \tag{1}$$

where f is a generalized variable that can represent variables such as voltage, current, or magnetic chain of the motor, and $T_{35/25}$ is the Clark transform matrix of coordinate variables of the form:

$$T_{3z/2z} = \begin{matrix} 1 & -\frac{1}{2} & -\frac{1}{2} \\ 0 & \frac{\sqrt{3}}{2} & \frac{\sqrt{3}}{2} \\ \frac{\sqrt{2}}{2} & \frac{\sqrt{2}}{2} & \frac{\sqrt{2}}{2} \end{matrix} \tag{2}$$

The inverse Clark transform, which realizes the transformation of two-phase $\alpha-\beta$ stationary coordinate variables to three-phase ABC natural coordinate variables, is given by:

$$\begin{bmatrix} f_A & f_B & f_C \end{bmatrix}^T = T_{2s/3s}\begin{bmatrix} f_\alpha & f_\beta & f_0 \end{bmatrix}^T \tag{3}$$

where $T_{2s/3s}$ is the inverse Clark transform matrix in the specific form:

$$T_{3z/2z} = T_{3z/2z}^{-1} = \begin{matrix} 1 & 0 & \frac{\sqrt{2}}{2} \\ \frac{1}{2} & \frac{\sqrt{3}}{2} & \frac{\sqrt{2}}{2} \\ \frac{1}{2} & -\frac{\sqrt{3}}{2} & \frac{\sqrt{2}}{2} \end{matrix} \tag{4}$$

For a three-phase symmetric system, f_0 is negligible in calculating the variables in the stationary coordinate system.

The Park transformation, which transforms the two-phase α-β stationary coordinate system variables to two-phase d-q synchronized rotating coordinate system variables. the Park transformation equation is:

$$\begin{bmatrix} f_d & f_q \end{bmatrix}^T = T_{2z/2r}\begin{bmatrix} f_\alpha & f_\beta \end{bmatrix}^T \tag{5}$$

where $T_{2s/2r}$ is the Park transformation matrix. Then:

$$T_{2s/2r} = \begin{bmatrix} \cos\theta_e & \sin\theta_e \\ -\sin\theta_e & \cos\theta_e \end{bmatrix} \tag{6}$$

The coordinate transformation of the two-phase $d-q$ synchronized rotating coordinate system to the two-phase $\alpha-\beta$ stationary coordinate system is called the inverse Park transformation, and the transformation equation is:

$$\begin{bmatrix} f_\alpha & f_\beta \end{bmatrix}^T = T_{2r/2s}\begin{bmatrix} f_d & f_q \end{bmatrix}^T \tag{7}$$

The expression for the inverse Park transformation matrix $T_2\tau/2s$ in Eq:

$$T_{2r/2s} = T_{2s/2r}^{-1} = \begin{matrix} \cos q_e & -\sin q_e \\ \sin q_e & \cos q_e \end{matrix} \tag{8}$$

In summary, the transformation relationship between the three-phase ABC natural coordinate system variables and the two-phase $d-q$ synchronized rotating coordinate system variables can be obtained as:

$$f_q \quad f_0 = T_{3z/2r}[f_A \quad f_B \quad f_C] \tag{9}$$

$$[f_A \quad f_B \quad f_C] = T_{2r/3} f_q \quad f_0{}^T \tag{10}$$

The coordinate transformation matrix in Eq:

$$T_{3z/2r} = T_{3z/2z}T_{2z/2r} \quad \frac{2}{3}\begin{matrix} \cos q_s & \cos(q_s - 2p/3) & \cos(q_s + 2p/3) \\ \sin q_s & -\sin(q_s - 2p/3) & -\sin(q_s + 2p/3) \\ 1/2 & 1/2 & 1/2 \end{matrix} \tag{11}$$

$$T_{2r/3z} = T_{3z/2r}^{-1} = \begin{matrix} \cos q_e & -\sin q_e & 1/2 \\ \cos(q_e - 2p/3) & -\sin(q_e - 2p/3) & 1/2 \\ \cos(q_e + 2p/3) & -\sin(q_e + 2p/3) & 1/2 \end{matrix} \tag{12}$$

2.1.2. PMSM mathematical modeling. Before establishing the mathematical model, the following assumptions are made:

1) The stator and rotor core magnetoresistance is neglected, and the eddy current and hysteresis loss are not counted.

2) The conductivity of the permanent magnet material is zero, and the permeability inside the permanent magnet is the same as that of air.

3) There is no damping winding on the rotor.

4) The excitation magnetic field generated by the permanent magnet and the armature reaction magnetic field generated by the three-phase winding are sinusoidally distributed in the air gap.

5) The waveform of induced electromotive force in the phase windings is sinusoidal during steady state operation.

Under the above assumptions, the mathematical model of PMSM in each coordinate system is established.

According to the method of coordinate transformation, the PMSM model in the three-phase stationary coordinate system is transformed into the model in the two-phase stationary coordinate system, and then the mathematical model of the PMSM in the $\alpha-\beta$-coordinate system can be obtained [16]. Namely:

$$\begin{bmatrix} i_a \\ i_\beta \end{bmatrix} = \begin{bmatrix} \frac{\sqrt{6}}{2} & 0 \\ \frac{\sqrt{2}}{2} & \sqrt{2} \end{bmatrix} \begin{bmatrix} I_A \\ I_B \end{bmatrix} \tag{13}$$

where i_a is the component of the stator current in the α-axis and i_s is the component of the stator current in the β-axis.

The PMSM voltage model in $\alpha-\beta$ coordinate system is:

$$\begin{bmatrix} U_a \\ U_\beta \end{bmatrix} = \begin{bmatrix} R_a + L_a p & 0 \\ 0 & R_a + L_\beta p \end{bmatrix} \begin{bmatrix} i_a \\ i_\beta \end{bmatrix} + \frac{\sqrt{6}}{2} \omega_r \psi_f \begin{bmatrix} -\sin\varphi \\ \cos\varphi \end{bmatrix} \tag{14}$$

where U_a is the stator voltage component in a axis, U_b is the stator voltage component in β axis, L_a, L_B is the inductance component of the motor in both axes respectively, and ω_r is the rotor's electrical angular velocity. The inductive components on the two axes satisfy the following relationship:

$$L_\alpha = L_\beta = \frac{3}{2} L_\varepsilon \tag{15}$$

Since the d-q coordinate system is rotating with the rotor, thus establishing the mathematical model of the PMSM in this coordinate system helps to analyze the dynamic and steady state performance of the whole control system of the PMSM, then the mathematical model of the PMSM in the d-q coordinate system is:

$$\begin{bmatrix} i_d \\ i_q \end{bmatrix} = \sqrt{\frac{2}{3}} \begin{bmatrix} \cos\varphi & \cos(\varphi - \frac{2\pi}{3}) & \cos(\varphi + \frac{2\pi}{3}) \\ -\sin\varphi & -\sin(\varphi - \frac{2\pi}{3}) & -\sin(\varphi + \frac{2\pi}{3}) \end{bmatrix} \begin{bmatrix} I_A \\ I_B \\ I_C \end{bmatrix} \tag{16}$$

where, i_d is the component of stator current in axis d and i_q is the component of stator current in axis q. Then:

$$\begin{bmatrix} i_d \\ i_q \end{bmatrix} = \begin{bmatrix} \frac{\sqrt{2}}{2}\sin\varphi + \frac{\sqrt{6}}{2}\cos\varphi & \sqrt{2}\sin\varphi \\ -\frac{\sqrt{6}}{2}\sin\varphi + \frac{\sqrt{2}}{2}\cos\varphi & \sqrt{2}\cos\varphi \end{bmatrix} \begin{bmatrix} I_A \\ I_B \end{bmatrix} \tag{17}$$

Similarly, the voltage equation of the PMSM in the d-q coordinate system is obtained as:

$$\begin{bmatrix} U_d \\ U_q \end{bmatrix} = \begin{bmatrix} R_i & 0 \\ 0 & R_i \end{bmatrix} \begin{bmatrix} i_d \\ i_q \end{bmatrix} + \begin{bmatrix} p & -\omega_r \\ \omega_r & p \end{bmatrix} \begin{bmatrix} \psi_d \\ \psi_q \end{bmatrix} \tag{18}$$

$$|U_s| = \sqrt{U_d^2 + U_q^2} \tag{19}$$

The magnetic chain equation is:

$$\begin{bmatrix} \psi_d \\ \psi_q \end{bmatrix} = \begin{bmatrix} L_d & 0 \\ 0 & L_q \end{bmatrix} \begin{bmatrix} i_d \\ i_q \end{bmatrix} + \psi_f \begin{bmatrix} 1 \\ 0 \end{bmatrix} \tag{20}$$

$$|\psi_z| = \sqrt{\psi_d^2 + \psi_q^2} \tag{21}$$

The torque equation is:

$$T = \frac{3}{2} p_a (\psi_d i_q - \psi_q i_d) \tag{22}$$

where U_d and U_q are the components of stator voltage in the d and q axes, ψ_d and ψ_q are the components of stator magnetic chain in the d and q axes, L_d and L_q are the components of stator inductance in the d and q axes, p_a is the number of pole pairs, and T is the torque of the permanent magnet synchronous motor.

2.2. *Permanent magnet synchronous motor switching control*

2.2.1. Basic idea of vector control. Permanent magnet synchronous motor as a nonlinear, strongly coupled, high-order multivariable system, each parameter in the motor is coupled with each other, so for the switching control of the permanent magnet synchronous motor has a strong nonlinearity.The basic idea of the switching vector control of the PMSM is to keep the base wave synthesized magnetic potential equivalent, mimic the idea of the speed control of the permanent magnet synchronous dc motor, and through the coordinate transformations, the three-phase currents of the motor, Voltage, magnetic chain converted to the rotor magnetic chain oriented two-phase reference coordinate system to decouple the physical quantities, respectively, the decoupled physical quantities to be controlled. That is to say, the excitation component and torque component of the stator current vector are controlled separately in the synchronous rotating coordinate system, and the switching vector control of the permanent magnet synchronous motor is achieved through such a transformation process.

2.2.2. Principle of the resonant pole inverter. The resonant pole inverter topology is shown in Fig. 1, which mainly consists of a rectifier circuit, an auxiliary resonant circuit, a driver circuit, and a permanent magnet synchronous motor [17]. The emitters of the auxiliary switches S_a, S_b, S_c are connected together so that only an additional gate drive power supply is required. The buffer capacitor C_{ra}, C_{rb}, C_{rc} slows down the voltage rise rate throughout the PMSM cycle and enables the three lower bridge arm switching tubes to be turned off at zero voltage, thus reducing the turn-off power loss and eliminating the turn-off voltage spikes. Before turning on the three lower bridge arm switching tubes, the corresponding auxiliary switches must be turned on to release the power in the snubber capacitor to zero so that the lower bridge arm switching tubes can be turned on at zero voltage. The common resonant inductor (L_r) is then utilized to resonate with the buffer capacitors connected in parallel with the lower bridge arm switching tubes to achieve zero voltage and zero current turn-on of the auxiliary switching tubes.

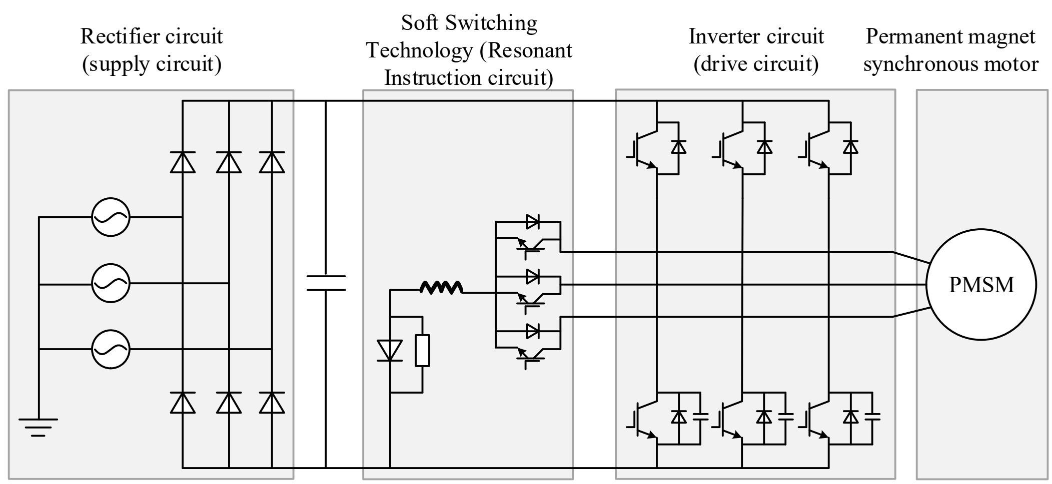

Fig. 1. Topology of resonant pole soft-switching inverter

For the convenience of analysis, the equivalent circuit of a particular switch can be obtained by taking a switching cycle in which switching tube V1 is kept constantly on, switching tube V6 operates under a PMSM modulation signal, and the rest of the switching devices are turned off. In the equivalent circuit, U_1 is the DC voltage source, u_{V_6} is the voltage on switching tube V_6, i.e., the voltage of buffer capacitor C_{rb}, and I_0 is the load current. Assuming that all devices are in ideal operation, the resonant inductance is much smaller than the load inductance, the load current at the transition moment of the switching state of the inverter bridge can be considered as a constant-current source, the operating modes of the circuit are described according to different moments, and the starting moment of each mode is taken as the zero moment of the mode. The details are as follows:

Mode 1 $(0 < t < t_1)$: Initial state, switching tube V_1 is closed, V_6 is disconnected, the load current flows through the continuity diode D_3, the terminal voltage u_{V_e} of switching tube V_6 is equal to the DC supply voltage U_1, and the resonant circuit does not work at this time.

Mode 2 $(t_1 < t < t_2)$: To turn on the switching tube V_6 with zero voltage, it is necessary to release the terminal voltage u_{v_e} to zero before that, so at the moment of t_i, the auxiliary switch S_b is closed, and under the action of the inductor, the current flowing through the inductor can not undergo a sudden change, realizing the auxiliary switch S_b with zero current turn on. The inductor current increases from zero, and the current on the continuity diode D_3 begins to decrease, the voltage and current expressions for the inductor are:

$$\frac{di_{L_r}}{dt} = \frac{U_1}{L_r} \tag{23}$$

This mode ends when the inductor current reaches the load current I_o. The duration is:

$$\Delta t_2 = t_2 - t_1 = \frac{L_t I_0}{U_1} \tag{24}$$

Mode 3 $(t_2 < t < t_3)$: At the moment of t_2, the current flowing through the continuity diode D_3 is zero, D_3 achieving zero-current shutdown, and thus solving the problem of D_3 reverse recovery currents that cause large losses. From moment t_2, i_{L_i} continues to increase, capacitor C_b and inductor L_t begin to resonate, C_{rb} discharges, and L_r is charged until the capacitor C_{tb} voltage decreases to zero when this mode ends. The expressions for the voltage u_v of the capacitor C_{tb} and the current i_{L_i} of the inductor are:

$$\begin{cases} u_{V_t}(t) = -L_t \dfrac{di_{L_t}}{dt} \\ i_{L_t}(t) = -C_t \dfrac{du_{V_t}(t)}{dt} + I_0 \end{cases} \tag{25}$$

where C_r is the value of capacitance C_r. The initial conditions are $u_V(0) = U_1$, $i_{L_i}(0) = I_0$, which simplifies to:

$$\begin{cases} u_{v_t}(t) = U_1 \cos(\omega_t t) \\ i_{L_t}(t) = I_0 + U_1 \sqrt{\dfrac{C_t}{L_t}} \sin(\omega_t t) \end{cases} \tag{26}$$

In the formula, $\omega_r = \sqrt{\dfrac{1}{C_r L_r}}$.

2.2.3. Strategy selection for vector control. Permanent magnet synchronous motor in operation will inevitably exist a certain amount of energy loss, and the various parts of the motor body will be due to the loss of heat generated by the overall temperature increases. When the motor structure switch is poorly designed, the increase in motor losses will lead to a sharp increase in heat production, reducing the life of the motor body, and the operating efficiency of the motor will also be reduced, which can be improved through reasonable switching control strategies. The vector control strategies commonly used for permanent magnet synchronous motors are $i_d = 0$ control, MTPA control, unit power factor control and so on.

Substituting $i_d = 0$ into the electromagnetic torque equation of the motor given before, it can be obtained:

$$T_e = \frac{3}{2} P_a \psi_f i_q \tag{27}$$

It can be seen that the electromagnetic torque output from the motor is only related to the motor q axis current i_q.

Under this control strategy, the magnitude and direction of the stator current i_s and the cross-axis current i_q are the same, the magnetic momentum space vector generated by the current vector is the same as the cross-axis direction, the magnetic chain space vector direction generated by the permanent magnets is the same as the straight-axis direction, and the phase relationship between the two is orthogonal. However, since the reluctance torque of the motor is zero in the control process, the permanent magnet synchronous motor is more widely used in the surface-mounted type, but the reluctance torque of the motor cannot be used in the built-in permanent magnet synchronous motor to improve the ability to carry loads, so in order to give full play to the advantages of the built-in type motor, and from the point of view of improving the efficiency of the system, the MTPA control strategy is usually adopted. Then:

$$T_e = \frac{3}{2} p_n \left[\psi_f i_s \sin\gamma + \frac{1}{2}(L_d - L_q) i_s^2 \sin 2\gamma \right] \tag{28}$$

When analysing the MTPA control strategy, it is necessary to obtain the trajectory of the motor stator current. During the operation of the motor, the stator current is affected by the motor windings and power device limits and can only vary within a certain area. The constraint that the motor stator current vector receives the influence of the motor windings can become the current limit circle, which is also the main constraint when the motor is operated in the interval below the rated speed, with the relation equation:

$$i_s = \sqrt{i_d^2 + i_q^2} \le i_{s_{max}} \tag{29}$$

where i_{s_max} is the maximum value of the motor stator current.

In addition to the current limit circle, the current vector trajectory is also limited by the voltage limit circle, which is given by the relation:

$$u_s = \sqrt{u_d^2 + u_q^2} \le u_{s_{-\max}} \tag{30}$$

where, u_{s_max} is the limit value of the motor inverter output voltage.

Then:

$$(L_d i_d + \psi_f)^2 + (L_q i_q)^2 \le \left(\frac{u_{s\_\max}}{\omega_q} \right) \tag{31}$$

The voltage limit circle is a cluster of ellipses defining the characteristic current I_{ch} as the coordinates of the centre point of the voltage limit circle. Then:

$$I_{ch} = -\frac{\psi_f}{L_d} \tag{32}$$

There is also a cluster of constant torque curves during the operation of the motor, and the current trajectory of the motor under the MTPA control strategy can be obtained by connecting the points with the smallest stator current vector amplitude on the constant torque curve.

3. Optimisation strategies for switching frequency control of permanent magnet synchronous motors

Permanent magnet synchronous motors have the advantages of low noise, high power density, etc., which can be widely used in aerospace, industrial production and other fields. The traditional control strategy is difficult to meet the requirements of high-performance motion control system due to low performance and poor anti-interference. The model predictive switching control strategy based on deep learning technology has become a research hotspot of permanent magnet synchronous motor switching control optimisation method due to its advantages of better dynamic performance and ease of adding various types of constraints. Based on this, this paper proposes a permanent magnet switch control optimization strategy based on fuzzy neural network PID controller, and combines the finite element model to analyse the temperature rise change of the permanent magnet switch under this strategy, which provides help for the efficient operation of permanent magnet synchronous motor.

3.1. Fuzzy Neural Network PID Controller

3.1.1. Incremental PID control. P, I, D in PID control algorithm are proportional, integral and differential respectively, which can realize proportional adjustment, integral adjustment and differential adjustment. In industrial manufacturing control, PID controller is widely used due to the advantages of simple structure, high stability and high reliability of the control algorithm. With the development of science and technology, PID control algorithms have been improved, among which there are incremental PID algorithms, which have been applied in the switching control system of permanent magnet synchronous motors [18]. Then:

$$u(k) = u(k-1) + \Delta u(k) \tag{33}$$

$$\Delta u(k) = K_p[e(k) - e(k-1)] + K_i e(k) + K_d[e(k) - 2e(k-1) + e(k-2)] \tag{34}$$

In the formula, $u(k)$ is the output signal of the controlled parameter at the moment of k, $u(k-l)$ is the output signal of the controlled parameter at the previous moment. $\Delta u(k)$ is the incremental change of the controlled parameter at the moment of k, K_p, K_i, K_d is the proportional, integral and differential gain respectively, $e(k)$ is the error of the current moment, $e(k-1)$ is the error of the previous moment, and $e(k-2)$ is the error of the earlier moment.

The incremental type does not need to add up all the deviations, but only needs to calculate the deviation of the last three times, this method has the characteristics of small calculation, low load on the controller, high calculation accuracy, small influence on the actuator, and when the system has large fluctuations, the influence on the adjustment of the control system is also relatively small.

3.1.2. Fuzzy Neural Networks. During system operation, temperature variations lead to fluctuations in system parameters such as stator resistance and inductance, and at the same time, permanent magnet synchronous motors tend to suffer from system modeling errors and are subject to external perturbations, and these uncertainties can degrade system performance. To cope with these negative effects and improve system robustness and immunity to perturbations, fuzzy neural networks (FNNs) with the ability of fuzzy systems to deal with fuzzy and uncertain information, as well as with the powerful nonlinear mapping and learning memory capabilities of neural networks, are introduced for approximating nonlinear unknown functions in the system with high accuracy [19].FNNs consist of defuzzification, knowledge base, defuzzification, and fuzzy reasoning, and are altogether divided into input layer, fuzzification layer, fuzzy inference layer and output layer.

Input Layer: $x_1, x_2, \cdots, x_M$ is the M input variables that feed into the fuzzy neural network. Each node in this layer represents an input variable and passes the input values directly to the next layer.

Fuzzification layer: in this layer, each node represents an affiliation function. The Gaussian function is chosen as the affiliation function for the fuzzification layer, therefore, the affiliation value for each input can be calculated as:

$$\wp_m^n = \exp\left(-\left(x_m - c_{mn}\right)^2 / d_{mn}^2\right) \tag{35}$$

Where $m = 1, 2, \cdots, M, n = 1, 2, \cdots, N$ is the total number of affiliation functions, c_{mn} and d_{mn} are the center and width values of the Gaussian function that fuzzifies the input linguistic variables.

Rule layer: this layer is responsible for executing the inference mechanism of the fuzzy logic system to accomplish fuzzy inference. Its inference process is based on nonlinear mapping through a series of IF-THEN rules. The normalized trigger value of the fuzzy logic system is calculated as using product inference, central averaging and single point fuzzy method:

$$S_n = \frac{\wp_m^n}{\sum_{m=1}^{M} \wp_m^n}, n = 1, 2, \cdots, N \tag{36}$$

Output layer: combining the output of the rule layer with the corresponding weight vector, the output of the FNN can be obtained as:

$$\hat{f} = W^T S \tag{37}$$

where $W = [W_1, W_2, \cdots, W_N]^\tau$ is the weight vector of the FNN and $S = [S_1, S_2, \cdots, S_M]^\tau$ is the basis function vector of the rule layer output.

According to the universal approximation theorem, an FNN with learning ability can approximate any continuous function $f(x)$ with arbitrary accuracy within a tight set Ω_x. Therefore, there exists an FNN with:

$$\sup_{x \in \Omega_x} | f(x) - W^T S | \leq \varepsilon(x) \tag{38}$$

The unknown optimal weight vector satisfies $W^* = \arg\min\left[\sup_{x \in \Omega_x} | f\left(x\right) - W^T S |\right]$, and in the subsequent controller design, the corresponding adaptive law will be designed to approximate the optimal weight W^* in combination with the adaptive theory. $\varepsilon(x)$ is the approximation error that satisfies $\varepsilon(x) < \bar{\varepsilon}$, and $\bar{\varepsilon} > 0$ is the upper bound of the approximation error.

3.1.3. PID controller design. The structural block diagram of the PMSM fuzzy neural network PID controller designed in this paper is shown in Fig. 2. As can be seen from the figure, the switching control system consists of two parts: the fuzzy neural network PID controller and the parameter recognizer, V^* refers to the given value of the control speed, and V refers to the actual output speed value of the PMSM. The fuzzy neural network PID controller consists of fuzzy neural network and incremental PID controller, the former will be based on the recognition of the speed error e and its error rate of change ec based on the algorithm for the calculation, and then the calculated parameter changes in the PID controller $\Delta k_p, \Delta k_i$ and Δk_d output, to achieve the adjustment of the various parameters of the PID controller. Finally, the fuzzy neural network control parameters are adjusted by the learning algorithm, and then the switching control of the permanent magnet synchronous motor is realized. The parameter recognizer is a learning algorithm that recognizes the Jacobian information of the PMSM and passes it to the fuzzy neural network.

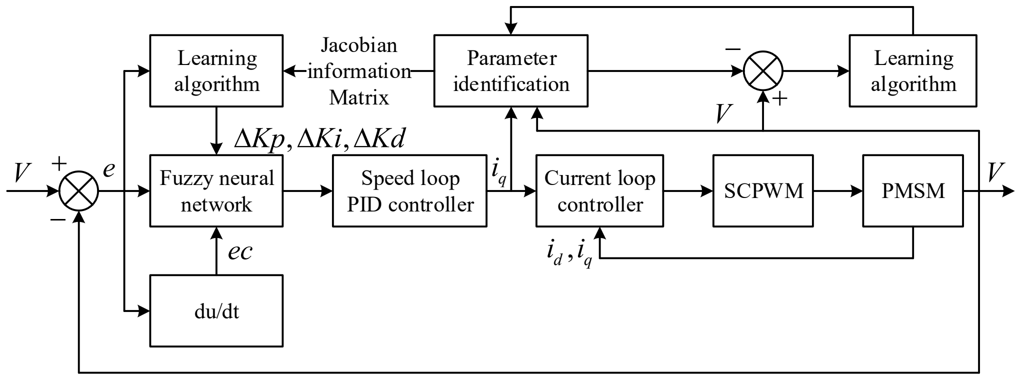

Fig. 2. Block diagram of PMSM FNN-PID switch control structure

3.2. Switch Simulation and Finite Element Modeling

3.2.1. Simulation Design of Permanent Magnet Switches. Modeling and analysis using simulation tools is an extremely critical step before validating the switching control system of a permanent magnet synchronous motor based on a resonant pole inverter.Both MATLAB/Simulink and PLECS are widely used simulation software in the research of permanent magnet synchronous motor control. Among them, MATLAB/Simulink has obvious advantages in algorithmic function implementation and embedded C code generation, while PLECS shows its unique expertise in analyzing electrical, thermal and magnetic characteristics in the field of power electronics. In this paper, PLECS software is used to co-simulate with MATLAB/Simulink and to construct a simulation model of a PMSM switching control system based on a resonant pole inverter.

The MATLAB/Simulink part mainly includes the coordinate transformation module, the FNN-PID control module and the MTPA control module.The PLECS part mainly includes the pulse width modulation module, the inverter topology circuit and efficiency calculation module and the motor and information acquisition module.

During the switching cycle, the switching device is not always on or off. Using the period average module Periodic Average and the period impulse average module Periodic Impulse Average, the conduction loss power and the switching loss power within the switching cycle can be calculated, respectively, wherein the module parameters need to be set to the values of the switching cycle. Further, in order to obtain the average loss power of the current fundamental cycle, it is necessary to add up the average loss power in each switching cycle, and then utilize the Periodic Impulse Average module for calculation, in which the module parameters should be set to the value of the current fundamental cycle. Similarly, the input power of the current fundamental cycle can be calculated using the cycle module.

3.2.2. Finite Element Modeling of Permanent Magnet Switches. COMSOL Multiphysics is a powerful finite element multi-physics simulation and analysis software, which provides a rich material library and predefined physical field equations, as well as a set of powerful built-in functions and operators. The software adopts the finite element analysis method, users can build multi-physics field models of electromagnetism, heat conduction and structural mechanics on the platform simultaneously or separately, users can select different physics field modules through the intuitive user interface, and flexibly combine them to solve specific problems. This software has the advantages of high accuracy, strong visualization, wide simulation, and fast simulation operation compared with the traditional numerical differential solution method and other finite element simulation software. Based on the switching control strategy of the permanent magnet synchronous motor proposed in this paper, the electric-thermal coupling module in COMSOL is used to analyze the simulation effect of temperature rise during the switching control process of the permanent magnet motor when the MTPA control strategy and FNN-PID control strategy are introduced respectively.

1) Motor solution domain modeling. The research object of this paper is a PS series model of permanent magnet synchronous motor provided by a manufacturer, and according to its datasheet, the parameter properties of the structural materials of each layer of the module can be derived. Then according to the dimensional parameters, combined with the actual physical characteristics of the module, the three-dimensional model of the permanent magnet synchronous motor switching control is established in COMSOL software as shown in Figure 3. By organizing the data related to the electrical and thermal properties of each layer of the simulation material of the module, the property parameters of its constituent material parts are set in COMSOL software to ensure the authenticity of the simulation results.

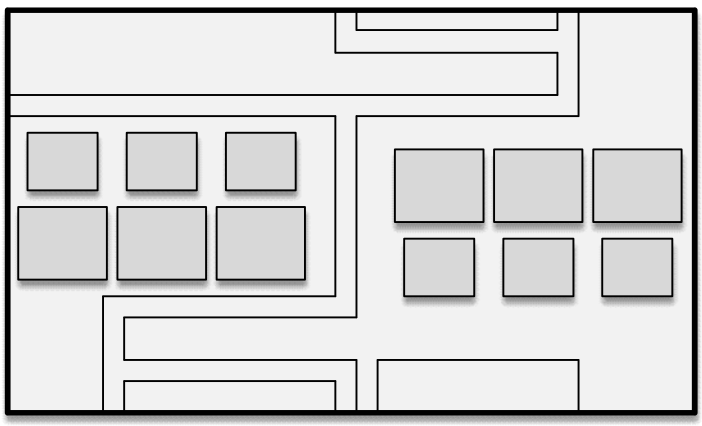

Fig. 3. 3D model of permanent magnet synchronous motor switch control

2) Mesh Segmentation. The purpose of finite element mesh splitting is to discretize the motor model, i.e., to split it into a finite number of cells. The results of finite element calculation are related to the number of grid sections, generally speaking, the more the number of grid sections, the more accurate the calculation results, but at the same time it will increase the calculation time, so the sparseness of the grid sections should be determined according to the needs of the motor components. In this paper, COMSOL software is used to perform grid dissection on the motor model, in which the number of nodes has 723680 and the number of cells has 2538490.

3) Basic assumptions. Before simulating and analyzing the temperature rise of the motor, the following basic assumptions are made in order to simplify the difficulty of the temperature field simulation and improve the work efficiency:

H1: Neglect the heat transfer between the motor case and the external air.

H2: Motor stator and rotor iron losses and winding copper losses are uniformly applied at the heat source.

H3: The effect of mechanical losses on the temperature field of the motor is neglected.

H4: The effect of temperature rise due to thermal radiation from the motor is neglected.

H5: Consider that the boundary conditions of the motor casing are consistent along the circumferential direction.

4) Determination of the heat dissipation coefficient on the outer surface of the casing. The outer surface of the enclosure undergoes natural convection heat transfer with air, and the average value of the heat dissipation coefficient h can be expressed as:

$$\begin{cases} h = N_u \dfrac{\lambda}{l} \\ N_u = C(G_r P_r)^n \\ G_r = \dfrac{g\alpha_v l^3 \Delta t}{v^2} \end{cases} \tag{39}$$

where, N_u is the Nussell coefficient, λ is the air thermal conductivity, l is the characteristic length, P_r is the Plante coefficient, G_r is the Gerashov number, C, n is the constant coefficient, which is generally taken as $C = 0.48, n = 0.25$. α_v is the coefficient of volumetric expansion, Δt is the convective heat transfer difference, and v is the kinematic viscosity of the air.

4. Validation of the effectiveness of switching control of permanent magnet synchronous motors

Permanent magnet synchronous motors are widely used in life and industry because of their simple structure, low manufacturing cost and high power density. In recent years, green energy-saving development is the development concept advocated by the state, and reducing the inverter switching frequency can not only reduce the switching loss, but also prolong the service life of the switch. Therefore, it is of great significance to study the control strategy of permanent magnet synchronous motor at low switching frequency. This chapter mainly focuses on the simulation analysis of the effectiveness of the FNN-PID switching control strategy given in the previous section, and explores the trend of the permanent magnet switch temperature rise under the switching control strategy in combination with finite elements, so as to lay a foundation for protecting the switching stability of the permanent magnet synchronous motor.

4.1. Validation of the permanent magnet switch control strategy

4.1.1. Performance in different operating states. In order to verify the performance of the permanent magnet synchronous motor system under the FNN-PID control method under high-speed and low-speed operating conditions, the permanent magnet synchronous motor system under the two control strategies of traditional MTPA and FNN-PID are simulated and compared under the same conditions respectively, and the response of the motor speed and torque are observed. The load torque is set to be 9N-m at startup, which changes to 16N-m and 8N-m at 0.2s and 0.8s, respectively, and the system is operated at a given speed of 1200rpm and 300rpm, respectively. The simulation results at a given speed of 1200 rpm are shown in Fig. 4, where Figs. 4(a)~(b) show the speed response curve and torque curve, respectively.

From Fig. 4, it can be seen that the speed of the FNN-PID switching control strategy can be stabilized quickly at high speeds, and the overshooting amount and start-up time are smaller than those of the traditional MTPA control strategy, and the speed is less affected when the load is disturbed, so it has a strong anti-disturbance capability. Under the traditional MTPA control strategy, the electromagnetic torque stabilizes around the given torque of 9N-m after about 0.08s of startup, and the torque pulsation is large. When using the FNN-PID control strategy, the electromagnetic torque stabilizes near the given torque of 9N-m after 0.03s of startup, and the electromagnetic torque fluctuates slightly after two load changes. However, the time needed to recover to stability is shorter, and the suppression of torque pulsation after stabilization is better, with better robustness.

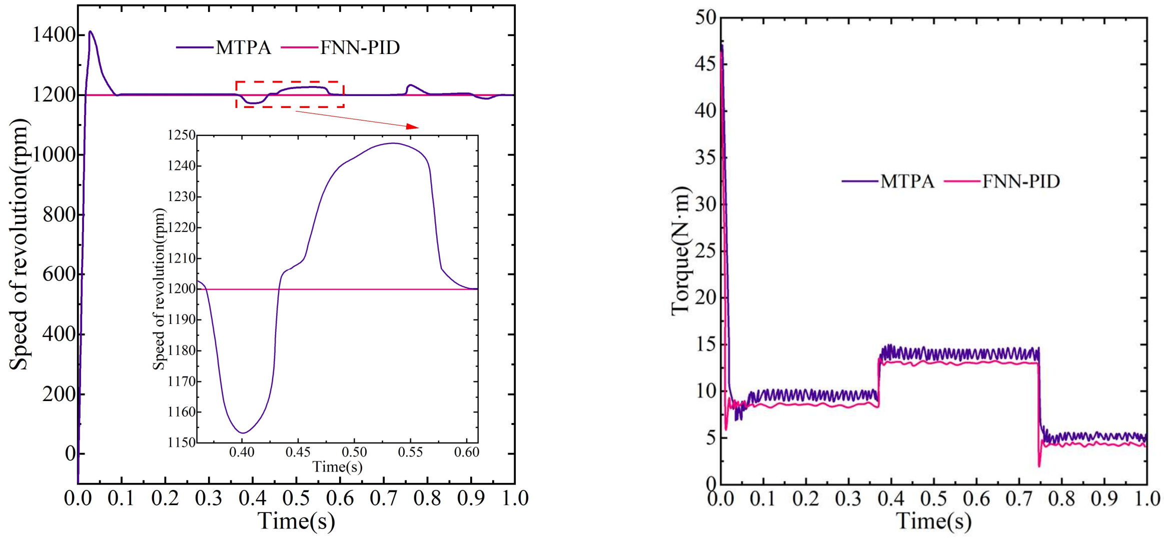

(a) Rotate speed curve

(b) Torque curve

Fig. 4. Simulation results for 1200rpm

The simulation results for a given speed of 300 rpm are shown in Fig. 5, where Fig. 5(a)~(b) shows the speed response curve and torque curve, respectively. During the low speed operation, the system speed of FNN-PID control strategy has almost no overshoot, and it stabilizes after reaching 300 rpm, the speed fluctuates when the load is disturbed, but the fluctuation amplitude is small, and the restoration of stabilization is faster than that of MTPA control strategy, and the dynamic response is better.The torque response of the FNN-PID control strategy is faster, and it can be stabilized at the set value quickly, and the amplitude of the torque pulsation is small.

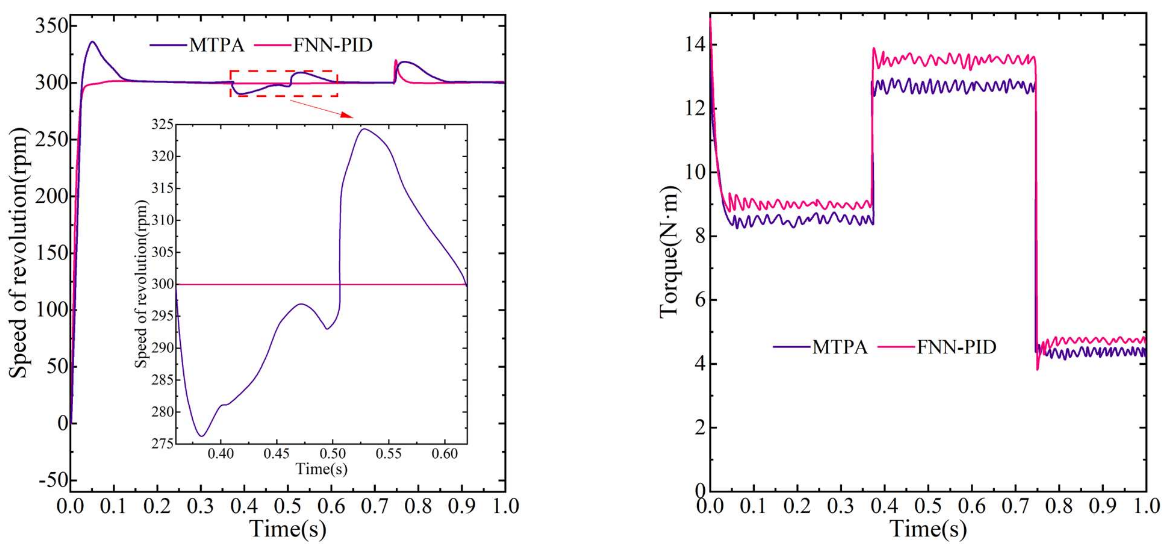

(a) Rotate speed curve

(b) Torque curve

Fig. 5. Simulation results for 300rpm

4.1.2. Comparison of steady state and dynamic performance:

1) Steady-state performance comparison. In the comparison experiments, the control period of both MTPA and FNN-PID control strategies is set to 120 μs, and the corresponding control frequency is

about 6.4 kHz, in which the supply voltage on the DC side of the inverter is 60 V, and the rotational speed of the motor is given as 200 rad/s. Fig. 6 shows the rotational speed, rotational torque, and motor phase current waveforms of the two control strategies in the steady state, in which Figs. 6(a)~(b) are the steady-state performances of the MTPA and FNN-PID control strategies, respectively.

In both control strategies, the rotational speed of the permanent magnet synchronous motor can achieve effective tracking of the given value, and the stator current has good sinusoidal degree, both of which show a more regular sinusoidal waveform. After actual measurements, the switching frequency of the PM synchronous motor corresponding to the MTPA control strategy is 1.427 kHz under such conditions, while the switching frequency of the PM synchronous motor supported by the FNN-PID control strategy is 1.084 kHz. Compared with the traditional MTPA PM switching control strategy, the optimized PM switching frequency of FNN-PID control strategy combining fuzzy neural network and incremental PID algorithm in this paper is reduced by 24.04%. Therefore, the FNN-PID control strategy can optimize the switching control of permanent magnet synchronous motors on the basis of ensuring the steady state performance of permanent magnet switching.

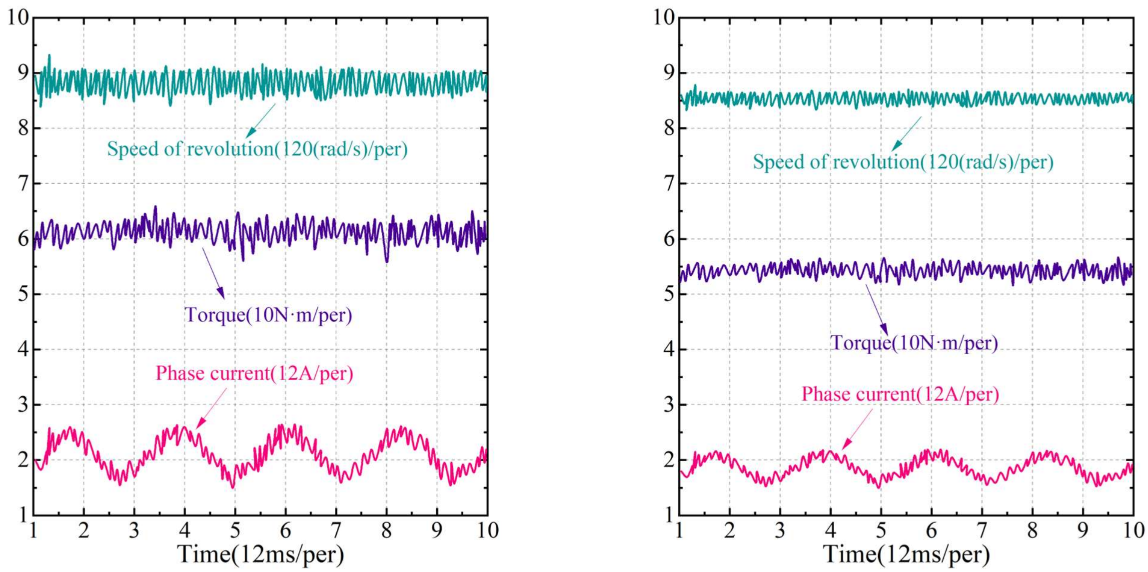

(a) MTPA (b) FNN-PID

Fig. 6. Experimental waveforms of steady performance

2) Dynamic performance comparison. Figure 7 shows the dynamic response waveforms of the two control strategies under the condition that the motor speed is stepped from 500 r/min to -500 r/min, and then stepped back to 500 r/min after 2 s. Among them, Figures 7(a)~(b) show the dynamic performances of the MTPA and FNN-PID control strategies, respectively. Comparing the experimental waveforms of the torque response of the two permanent magnet synchronous motor switching control strategies, it can be seen that the torque response time of both of them is about 2.2ms, and the speed tracking accuracy of the MTPA control strategy is 4.38%, and the speed tracking accuracy of the FNN-PID control strategy is 4.61%. It can be seen that the FNN-PID control strategy, which combines the deep learning algorithm and the incremental PID algorithm, maintains the good dynamic performance of the direct torque control in the switching control of permanent magnet synchronous motor. The FNN-PID control strategy suppresses the common mode voltage and increases the torque fluctuation at the same time, so the FNN-PID control strategy is more suitable for applications that emphasize on reliability. However, compared with the MTPA control strategy, the torque fluctuation of the FFNN-PID control strategy only increases by about 1/6, while the common-mode voltage is basically completely suppressed. Therefore, considering the reliability and the control accuracy, the FFNN-PID control

strategy is significantly better than the MTPA switching control strategy when switching control of the permanent magnet synchronous motor is carried out.

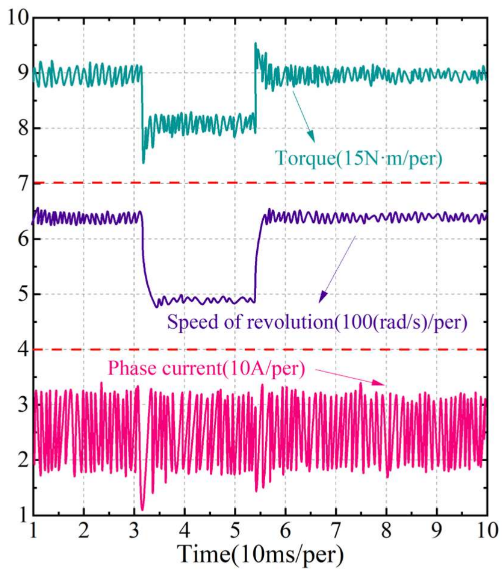

(a) MTPA

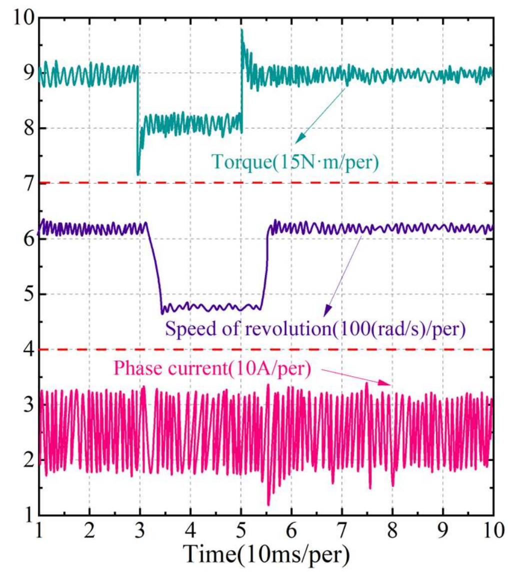

(b) FNN-PID

Fig. 7. Experimental waveforms of dynamic performance

4.1.3. Verification of Average Switching Frequency:

1) Average switching frequency curve. In order to verify the effectiveness of the FNN-PID control strategy proposed in this paper in performing switching control of permanent magnet synchronous motor, MTPA and fixed weight coefficients (GD-MPC) are selected as a comparison, and the average switching frequency curves under different control modes are obtained as shown in Fig. 8, where Figs. 8(a) to (b) are the average switching frequency and the fuzzy weight coefficients under the speed variation, respectively.

In the MTPA control strategy, the average switching frequency is about 16.28 kHz at a speed of 400 r/min, and the average switching frequency is about 11.65 kHz at a speed of 1600 r/min. In the GD-MPC control strategy, the average switching frequency fluctuates between 6 and 9 kHz at a speed of 400 r/min, and the average switching frequency is about 9.57 kHz at a speed of 1600 r/min. In the FNN-PID control strategy, the average switching frequency fluctuates between 5.82 kHz at 400 r/min and 9.12 kHz at 1600 r/min, and the switching term weighting coefficient fluctuates between 0.28 and 0.28 at 400 r/min, and the switching term weighting coefficient fluctuates between 0.28 and 0.28 at 1600 r/min, and the switching term weighting coefficient fluctuates between 0.28 and 0.28 at 400 r/min, and it is 0.28 at 1600 r/min when the speed changes abruptly. /min, the switching term weighting coefficient decreases to about 0.21.

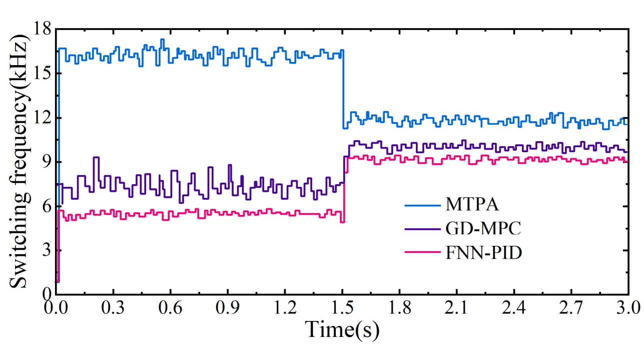

(a) Average switching frequency

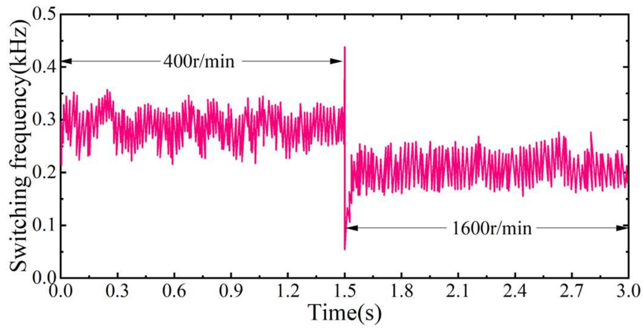

(b) Fuzzy weight coefficient

Fig. 8. Simulation result under speed change

2) Permanent magnet synchronous motor with load test. The conventional MTPA control strategy and FNN-PID control strategy are respectively used to carry out the load test on the 35Hz permanent magnet motor, and the results of the permanent magnet synchronous motor load test data are shown in Fig. 9. It can be seen that compared with the conventional MTPA control strategy, the PM synchronous motor with FNN-PID control strategy can reduce the switching control loss of up to 0.293W when carrying a light load of 100mN*m. With the increase of load, the switching control loss can also be reduced by 0.108W at 240mN*m with heavy load. The experimental results verify the effectiveness of the FNN-PID control strategy when applied to the switching control of permanent magnet synchronous motors. The FNN-PID control strategy can reduce the switching loss of the drive and further reduce the overall loss of the drive at the frequency point of 35Hz for the performance evaluation of permanent magnet synchronous motors.

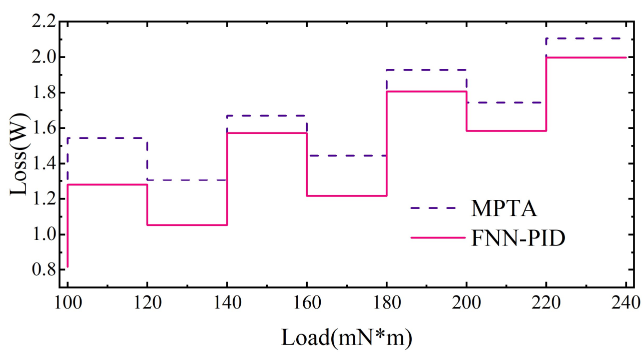

Fig. 9. The loss comparison of the controller

4.2. Simulation analysis of temperature rise of permanent magnet switch

4.2.1. Rated operating condition temperature rise test. The test permanent magnet synchronous motor is mounted on the dynamometer stand, connected to the high and low voltage wiring harness, oil pipe, temperature acquisition equipment, etc. The test motor is a special prototype, with small holes in the stator slot, and temperature sensors on both sides of the winding end and the winding in the stator slot.

Based on the finite element model of the permanent magnet synchronous motor established in the previous section, take 1500r/min, 60N·m working condition as an example, run for 20min to reach thermal equilibrium, and then test the maximum temperature trend of the winding in the interval of 1000r/min, 60N·m rated torque condition, as shown in Table 1. The highest temperatures are found in the stator slot. From the above results, it can be seen that the difference between the maximum temperature of the measured winding and the maximum temperature of the calculated winding under the rated condition is less than 9℃, and the finite element calculation model under the switching control support of the permanent magnet synchronous motor given in this paper has a certain degree of accuracy. In summary, the finite element model calculates the winding temperature with the measured comparison trend is consistent, and the maximum error between the two does not exceed 9 ℃, the general motor calculation temperature error between 4.5% and 9.5% or error less than 9 ℃, can meet the needs of the actual project. Therefore, the finite element calculation model of permanent magnet synchronous motor designed in this paper has a certain degree of accuracy and can significantly reflect the temperature rise change of the motor under switching control.

Table 1. The measured temperature is compared with the calculation temperature

Speed (r/min)	Torque (N·m)	Power (kW)	Calculated (℃)	Measured (℃)	Error (℃)
1500	60	10.42	122.48	118.51	3.97
2500	60	20.53	133.57	126.74	6.83
3500	60	31.19	135.28	132.43	2.85
4500	60	40.85	141.06	136.25	4.81
5500	60	51.38	150.47	141.69	8.78
6500	60	62.74	154.83	147.38	7.45
7500	60	71.97	156.92	150.46	6.46
8500	60	82.62	159.41	152.57	6.84
9500	60	90.05	161.35	157.63	3.72
10500	60	100.17	162.78	159.34	3.44

4.2.2. Temperature rise curves before and after optimization. The purpose of permanent magnet switching control is to ensure that the permanent magnet synchronous motor generates minimum loss during operation, and to ensure that the temperature variation of the permanent magnet synchronous motor is within a reasonable range, so that the permanent magnet synchronous motor can operate stably. Based on this, the finite element model established in the previous section is used to test the temperature rise curves of the rotor permanent magnets of the permanent magnet synchronous motor before and after the optimization of the FNN-PID control strategy, so as to clarify the effectiveness of the control strategy applied to the switching control of the permanent magnet synchronous motor. Figure 10 shows the transient temperature curve changes of the permanent magnet rotor before and after optimization, and Table 2 shows the temperature comparison of each winding of the permanent magnet synchronous motor before and after optimization.

When the motor is running at rated load, there is basically no eddy current loss in the rotor permanent magnets. The temperature rise of the rotor permanent magnet mainly comes from the heat transfer of the stator winding. Before the implementation of permanent magnet switching control optimization, eddy currents are induced in the permanent magnets, generating eddy current losses; at this time, the temperature rise of the permanent magnets comes from eddy current losses and heat transfer from the stator windings. After the switching control of the permanent magnet synchronous motor, the change rule of the temperature field is the highest temperature near the windings, and compared with the pre-optimization, the temperature is reduced by about 31.99%, and the temperature of the neighboring side windings is reduced by 32.29℃. Before the optimization of switching control, the rotor permanent magnet is affected by the increase of eddy current loss and stator winding heat transfer, and the temperature reaches up to 76.75℃. The temperature was reduced from 62.56°C to 47.68°C by the distance of the rotor from the heat source. The main heat source causing the temperature rise of the motor before carrying out permanent magnet switching control is the winding copper consumption of the faulty winding, and the heat is transferred to all parts of the motor through the air gap, which increases the overall temperature of the motor. The permanent magnet switching control can significantly reduce the temperature of the air gap, thus slowing down the rate of increase of the motor temperature rise curve.

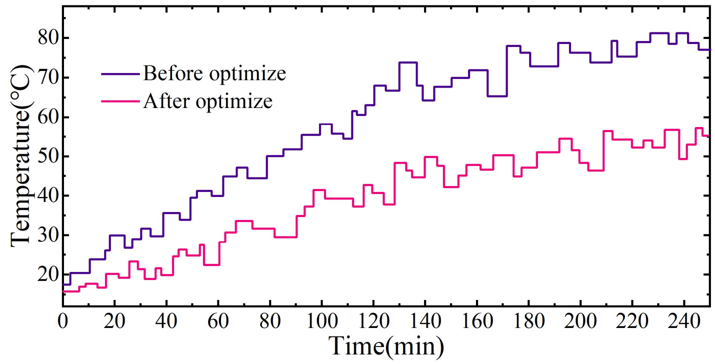

Fig. 10. The temperature rise curve before and after optimization

Table 2. Temperature contrast before and after optimization

Module	Before optimize (℃)	After optimize (℃)
Winding	107.69	73.24
Adjacent winding	104.48	72.19
Side winding	99.17	72.19
Air gap	85.32	61.51
Permanent magnet	76.75	54.43
Rotor	62.56	47.68

In addition, the room temperature of about 25.5ºC was captured using Fluke software, and after 20 min of stable operation of the system, the surface temperature of the device reached 45.28ºC with the traditional MTPA control strategy, while the surface temperature of the device with the FNN-PID control strategy was only 34.19ºC, which reduced the temperature rise significantly. In addition, due to the reduction of the switching frequency, the permanent magnet switching loss of the FNN-PID control strategy is reduced by about 35% compared with the traditional vector control. It can be seen that the FNN-PID control strategy proposed in this paper can effectively reduce the switching frequency of the system and the temperature rise of the system converter on the premise that it has similar control performance to its current loop compared to the traditional MTPA control strategy, which lays the foundation for further improving the control stability and reliability of the permanent magnet synchronous motor inverter system.

5. Conclusion

The article proposes a permanent magnet switch control optimization strategy based on deep learning, and analyzes the change of temperature rise under this control strategy with a finite element model. Based on the simulation results, the following conclusions are drawn:

1) Under the MTPA control strategy, the electromagnetic torque stabilizes near the given torque of 9N-m after about 0.08s of startup, and the torque pulsation is large. With the FNN-PID control strategy, the electromagnetic torque stabilizes around the given torque of 9N-m after 0.03s of startup.

2) The switching frequency of the PM synchronous motor under the FNN-PID control strategy is 1.084 kHz, which is 24.04% lower than that of the MTPA PM switching control strategy. In the FNN-PID control strategy, the average switching frequency is at about 5.82kHz, 9.12kHz when the speed is 400r/min and 1600r/min respectively.

3) The difference between the measured maximum winding temperature and the calculated

maximum temperature under the rated operating condition is less than 9°C. The finite element calculation model under the switching control support of the PM synchronous motor given in this paper has a certain degree of accuracy, and the PM switching loss with the FNN-PID control strategy is reduced by about 35% relative to the traditional MTPA control strategy.

In conclusion, the use of deep learning and finite element analysis can realize the optimal design of the permanent magnet switch control, which can help to promote the stable operation of the permanent magnet synchronous motor and enhance the service life of the permanent magnet synchronous motor.

References

[1] Cho, D. J., Woo, D. K., Ro, J. S., Chung, T. K., & Jung, H. K. (2013). Novel electromagnetic actuator using a permanent magnet and an inter-locking mechanism for a magnetic switch. IEEE Transactions on Magnetics, 49(5), 2229-2232.

[2] Sabzkouhi, A. M., & Haghighi, A. (2018). Uncertainty analysis of transient flow in water distribution networks. Water Resources Management, 32, 3853-3870.

[3] Zhan, J., Liu, W., Chung, C. Y., & Yang, J. (2020). Switch opening and exchange method for stochastic distribution network reconfiguration. IEEE Transactions on Smart Grid, 11(4), 2995-3007.

[4] Li, B., He, J., Li, Y., & Li, R. (2018). A novel solid-state circuit breaker with self-adapt fault current limiting capability for LVDC distribution network. IEEE Transactions on Power Electronics, 34(4), 3516-3529.

[5] Salman, H. M., Pasupuleti, J., & Sabry, A. H. (2023). Review on Causes of Power Outages and Their Occurrence: Mitigation Strategies. Sustainability, 15(20), 15001.

[6] Srivastava, I., Bhat, S., Vardhan, B. S., & Bokde, N. D. (2022). Fault detection, isolation and service restoration in modern power distribution systems: A review. Energies, 15(19), 7264.

[7] Tang, L., & Luan, S. (2023). Cosimulation of Bistable Permanent Magnet Circuit Breakers. IEEE Transactions on Industrial Electronics, 71(3), 2800-2809.

[8] Jooshaki, M., Karimi-Arpanahi, S., Lehtonen, M., Millar, R. J., & Fotuhi-Firuzabad, M. (2020). Reliability-oriented electricity distribution system switch and tie line optimization. IEEE Access, 8, 130967-130978.

[9] Ditmanson, C., Hein, P., Kolb, S., Mölck, J., & Bernet, S. (2014). A new modular flux-switching permanent-magnet drive for large wind turbines. IEEE Transactions on Industry Applications, 50(6), 3787-3794.

[10] Drzewosz, A., & Wolny, S. (2024). The problem of stability in mechanical systems using the example of mine hoist installations. Applied Sciences, 14(15), 6472.

[11] Yakovlev, V. L., Glebov, A. V., Bersenyov, V. A., Kulniyaz, S. S., & Ligotskiy, D. N. (2020). Influence of an installation angle of the conveyor lift on the volumes of mining and preparing work at quarries at the cyclic-flow technology of ore mining. News of the National Academy of Sciences of the Republic of Kazakhstan. Series of Geology and Technical Sciences, 4(442), 127-137.

[12] Ilcea, G. I., Molnar, R. N., Pasculescu, D., Marioane, A. C., Lazar, T., Andreica, M., & Furdui, D. (2023, October). Device for Controlling the Mining Elevator Transportation Process. In International Conference Interdisciplinarity in Engineering (pp. 204-213). Cham: Springer Nature Switzerland.

[13] Huang, J., Luo, C., Yu, P., & Hao, H. (2020). A methodology for calculating limit deceleration of flexible hoisting system: A case study of mine hoist. Proceedings of the Institution of Mechanical Engineers, Part E: Journal of Process Mechanical Engineering, 234(4), 342-352.

[14] Jiang, J., Lin, H., & Fang, S. (2017). Optimization design of a permanent magnet actuator for 126-kV vacuum circuit breaker. IEEE Transactions on Applied Superconductivity, 28(3), 1-5.

[15] Binghao Yu,Yiming Hu & Dequan Zeng. (2024). Study on Mathematical Models for Precise Estimation of Tire–Road Friction Coefficient of Distributed Drive Electric Vehicles Based on Sensorless Control of the Permanent Magnet Synchronous Motor. Symmetry(7),792-792.

[16] Zuo Shuguang,Huang Zhiyong,Wu Zhipeng & Liu Chang. (2023). Improved Mathematical Model and Modeling of Permanent Magnet Synchronous Motors Considering Saturation, Spatial Harmonics, Iron Loss and Deadtime Effect. Arabian Journal for Science and Engineering(5),6939-6955.

[17] Kasun Peiris,Sean Elphick,Jason David & Duane Robinson. (2025). Characterisation of Harmonic Resonance Phenomenon of Multi-Parallel PV Inverter Systems: Modelling and Analysis. Energies(2), 443-443.

[18] Hanzhen Xiao,Guanyu Lai,Yun Zhang,Dengxiu Yu & C.L. Philip Chen. (2024). Incremental swarm coordination control with self-triggered-organized topology and predictive-based control method. Information Sciences120969-120969.

[19] Weiwei Jiang,Yafeng Zhan & Xin Fang. (2025). Fuzzy neural network based access selection in satellite–terrestrial integrated networks. Journal of Network and Computer Applications104108-104108.